Electronic Supplementary Information

A multi-interface CoNi-SP/C heterostructure for quasi-solid-state hybrid supercapacitor with a graphene oxide-containing hydrogel electrolyte

Zixiao Li[a], Chenchen Ji[a,*], Fengjiao Guo[a], Hongyu Mi[a,*], Xiaoqing Zhu[a], Jieshan Qiu[b,*]

[a] School of Chemical Engineering and Technology, Xinjiang University, Urumqi 830046, Xinjiang, People's Republic of China

[b] State Key Laboratory of Chemical Resource Engineering, College of Chemical Engineering, Beijing University of Chemical Technology, Beijing 100029, People's Republic of China

*Corresponding author. E-mail: Hongyu Mi, mmihongyu@163.com; Chenchen Ji, jichenchen2010@163.com; Jieshan Qiu, qiujs@mail.buct.edu.cn

1. Experimental Section

1.1. Preparation of CoNi-MOF

CoNi-MOF precursor was prepared by a reported solvothermal method.[1] Typically, 1 mmol $Co(NO_3)_2 \cdot 6H_2O$ and 1 mmol $Ni(NO_3)_2 \cdot 6H_2O$ were dissolved in 30 mL N, N-dimethylformamide (DMF) under ultra-sonication for 0.5 h. Then, 0.1 g polyvinylpyrrolidone (PVP, MW 58000) and 150 mg trimesic acid (H_3BTC) were added into the above salt-containing organic solvent under magnetic stirring for another 0.5 h. After that, the solvent was poured into 50 mL Teflon-lined stainless-steel autoclave and heated at 150 °C for 6 h. The final CoNi-MOF was washed with ethanol for several times, and dried at 60 °C.

1.2. Preparation of CoNi-SP/C, CoNi-P/C, and CoNi-S/C.

CoNi-SP/C was synthesized by chemical vapor deposition (CVD). 20 mg CoNi-MOF and 200 mg mixed $NaH_2PO_2 \cdot H_2O$ and thiourea (mass ratio is 1:2) were located downstream and upstream of the tube furnace. The reaction was performed at 350 °C for 2 h with a speed of 2 °C min^{-1}.[2] CoNi-P/C and CoNi-S/C were synthesized by the same method but without thiourea or $NaH_2PO_2 \cdot H_2O$.

1.3. Preparation of PVA/PAM/GO

Firstly, 7 mg graphene oxide (GO) was dispersed in 7 mL deionized water by ultra-sonication, then 1 g PVA was dissolved into the above solution at 90 °C for 1 h. After that, 2.1 g acrylamide (AM) monomer, 0.0662 g (2-Hydroxy-4'-(2-hydroxyethoxy)-2-methylpropiophenone), and 1.36 mg N, N'-methylenebisacrylamide (MBA) were added into the PVA/GO suspension and stirred for 10 min. Subsequently, the above mixture was poured into the mold, and stood for 1 h under UV irradiation (λ= 365 nm wavelength, intensity of 8 W), finally obtaining the PVA/PAM/GO hydrogel.

1.4. Materials Characterization

Scanning electron microscopy (SEM, SU-8010) was employed to study the morphologies of various products. Their microstructures were made clear by employing transmission electron microscopy (TEM, 2100F). The phase feature was verified via X-ray diffraction (XRD, Brüker D8 advance), and the elemental components were clarified by X-ray photoelectron spectroscopy (XPS, Thermo Fisher ESCALAB 250Xi). Nitrogen adsorption-desorption apparatus (BSD-PS (M)) was employed for the surface area and pore structure based on the Brunauer-Emment-Teller (BET) method and the nonlocal density functional theory (NLDFT). A Brüker VERTEX70 Fourier transform infrared (FTIR) spectrometer was used to investigate the chemical components.

1.5. Electrochemical Evaluation

Electrochemical tests were carried out by cyclic voltammetry (CV), galvanostatic charge–discharge (GCD), and electrochemical impedance spectroscopy (EIS) using a CHI660b electrochemical workstation. The cycling durability was examined on a CT2001A LAND tester. The performance of the samples was examined in a conventional three-electrode setup using the Pt counter electrode, Hg/HgO reference electrode, and 2.0 M KOH aqueous electrolyte. Prior to the measurements, the working electrode (WE) based on the obtained sample was prepared by mixing active material, acetylene black, and polytetrafluoroethylene (mass ratio = 8:1:1) in ethanol. The dried mixture was rolled into the sheet, cut into several small sheets, and pressed on the Ni current collector (with the mass loading of 2.5 mg cm^{-2}). The gravimetric capacities (Q_g, C g^{-1}) of the samples were calculated from GCD curves using the following equation:[3]

$$Q_g = \frac{2I\int V\mathrm{d}t}{mV} \quad (1)$$

where I (A) stands for the discharge current, $\int V\mathrm{d}t$ (V s) is the integral area under a discharge curve, m (g) is the mass of the active electrode material, and V (V) is the potential window. Electrochemical impedance spectroscopy (EIS) tests were recorded in the frequency range of 10^5–10^{-2} Hz. In HSC devices, the mass ratio of active materials in both electrodes was determined based on the charge balance using the formula below:[4]

$$\frac{m_+}{m_-} = \frac{Q_{g-}}{Q_{g+}} \quad (2)$$

where m (g) is the mass of the active electrode material, and Q_g (C g^{-1}) is the gravimetric capacity. The CoNi-SP/C to AC mass ratio is equal to 1:2.5 in the HSC. The gravimetric capacity (Q_{cell}, C g^{-1}), energy density (E, Wh kg^{-1}), and power density (P, W kg^{-1}) of the devices were calculated using the formulas below:[5]

$$Q_{cell} = \frac{2I\int V\mathrm{d}t}{mV} \quad (3)$$

$$E = \frac{I\int V\mathrm{d}t}{3.6m} \quad (4)$$

$$P = \frac{3600E}{t} \quad (5)$$

where m (g) is the total mass of both active electrode materials, V (V) is the discharge voltage, and t (s) is the discharge time.

2. Results and discussion

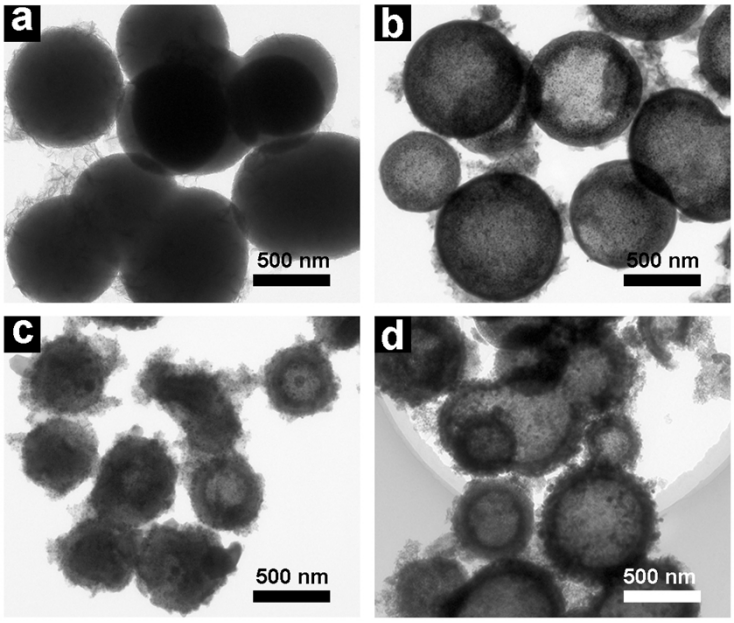

Fig. S1 TEM images of (a) CoNi-MOF, (b) CoNi-P/C, (c) CoNi-S/C, (d) CoNi-SP/C.

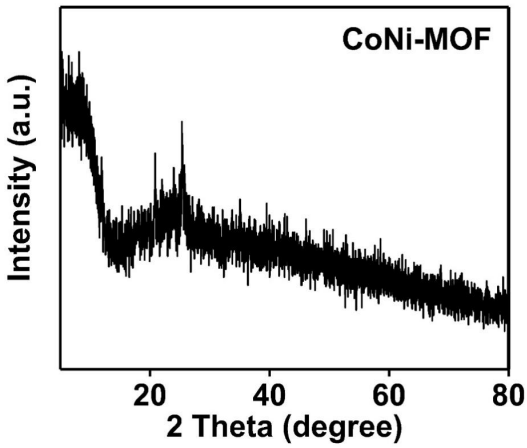

Fig. S2 XRD pattern of CoNi-MOF.

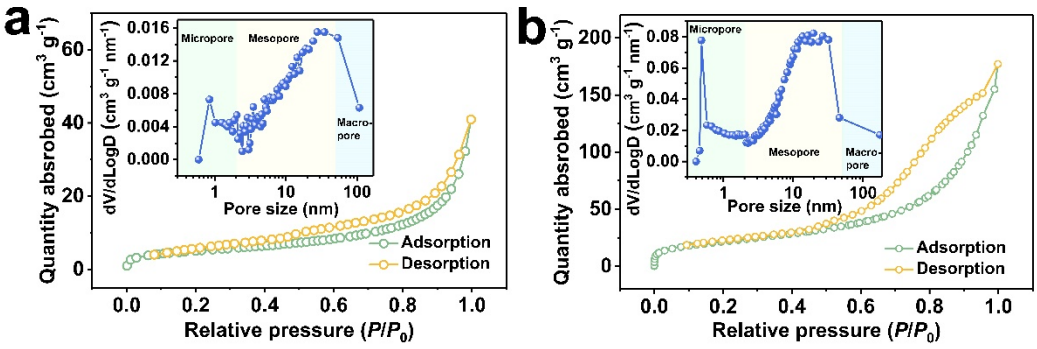

Fig. S3 Nitrogen adsorption-desorption isotherms and the corresponding pore size distributions (insets) of (a) CoNi-P/C and (b) CoNi-S/C.

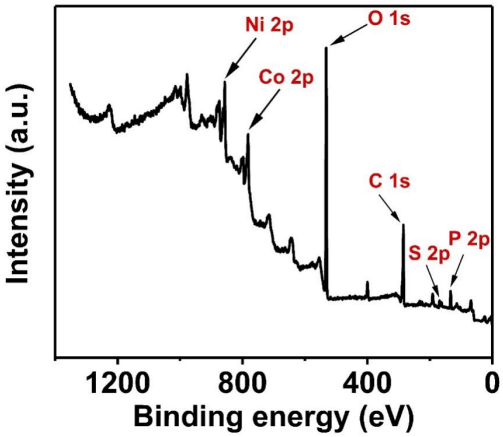

Fig. S4 XPS survey spectrum of CoNi-SP/C.

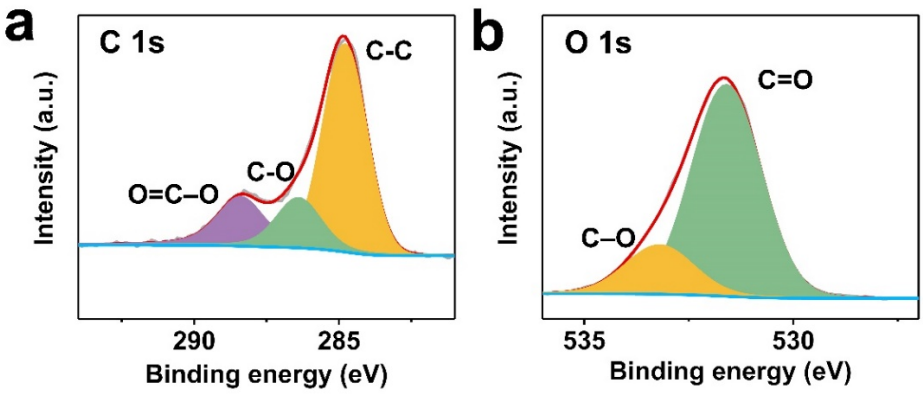

Fig. S5 XPS spectra of (a) C 1s and (b) O 1s for CoNi-SP/C .

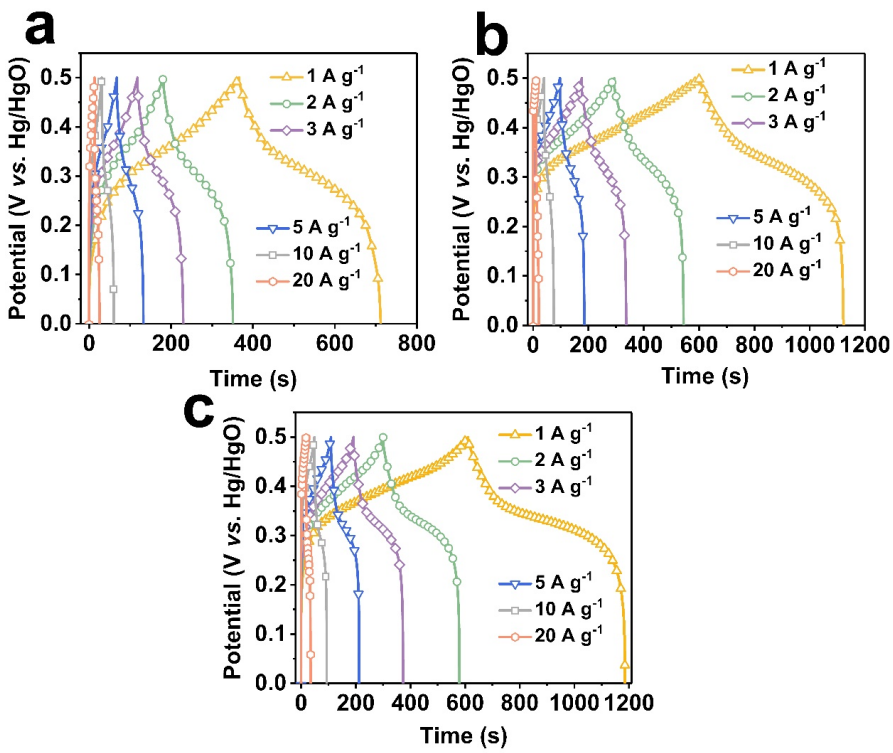

Fig. S6 GCD curves of (a) CoNi-P/C, (b) CoNi-S/C, and (c) CoNi-SP/C electrodes at 1−20 A g^{-1}.

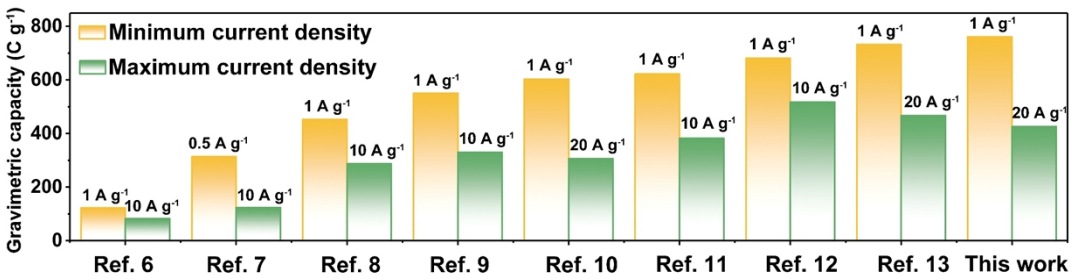

Fig. S7 The capacity comparison of CoNi-SP/C with other published electrode materials.

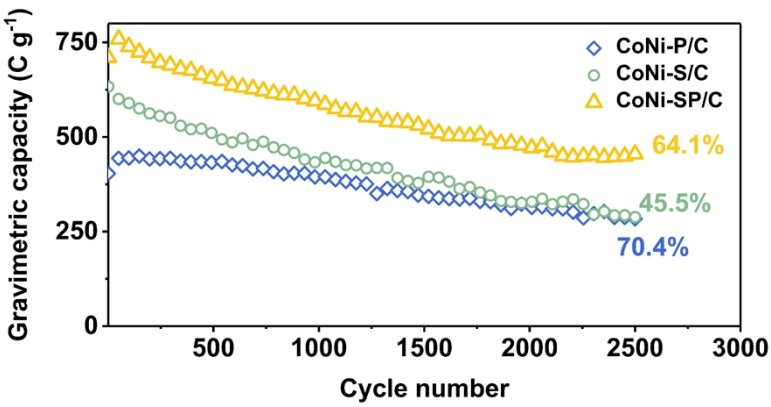

Fig. S8 Cycling stability for CoNi-P/C, CoNi-S/C, and CoNi-SP/C electrodes.

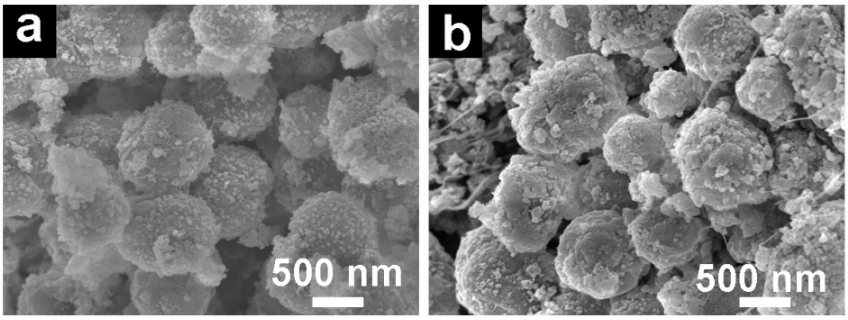

Fig. S9 SEM images of CoNi-SP/C (a) before and (b) after cycling.

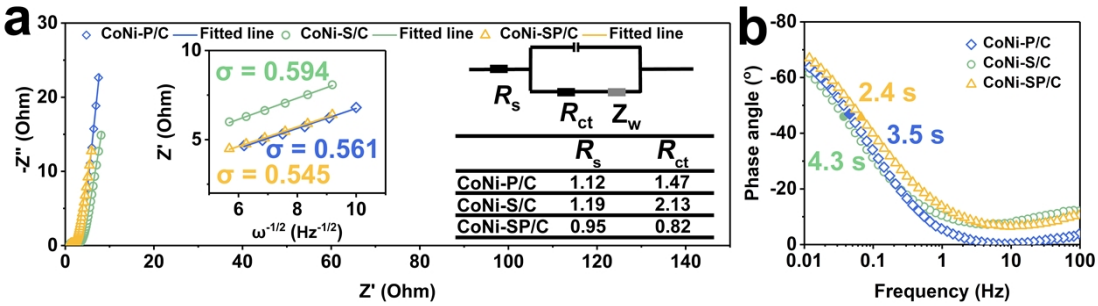

Fig. S10 (a) EIS plots of CoNi-P/C, CoNi-S/C, and CoNi-SP/C electrodes. Insets indicate the Z' vs. $\omega^{-1/2}$ plots in the low frequency range, fitted equivalent circuit, and resistance results. (b) The phase angle vs. frequency plots of CoNi-P/C, CoNi-S/C, and CoNi-SP/C electrodes.

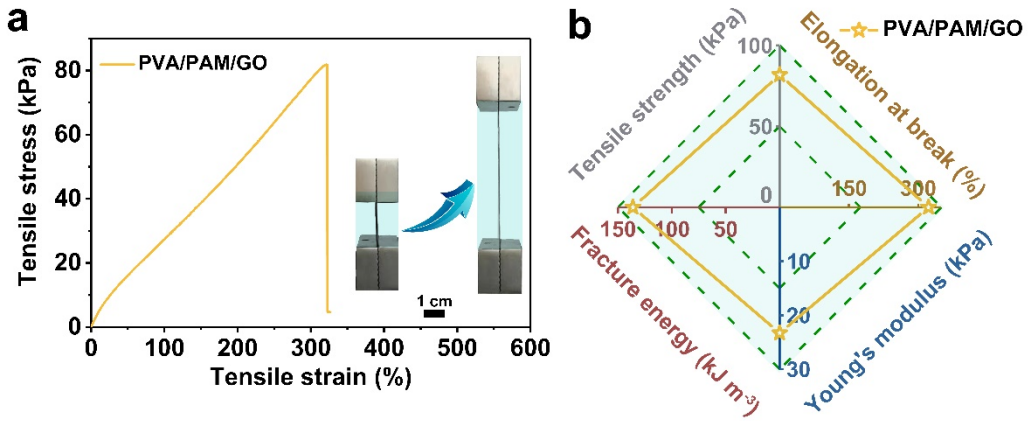

Fig. S11 (a) Tensile stress–strain curves of the PVA/PAM/GO hydrogel. (b) The mechanical properties in terms of tensile strength, elongation at break, fracture energy, and Young's modulus of the PVA/PAM/GO hydrogel.

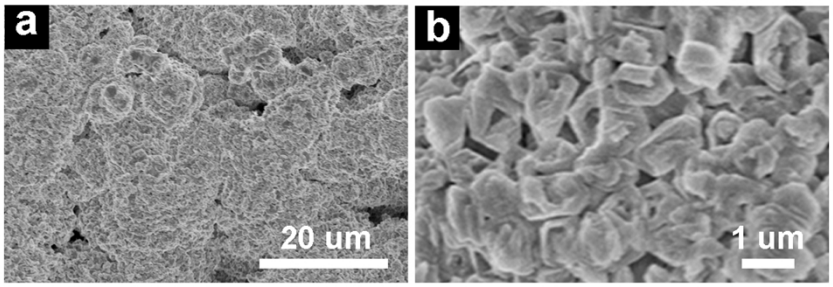

Fig. S12 SEM images of the PVA/PAM/KOH hydrogel electrolyte.

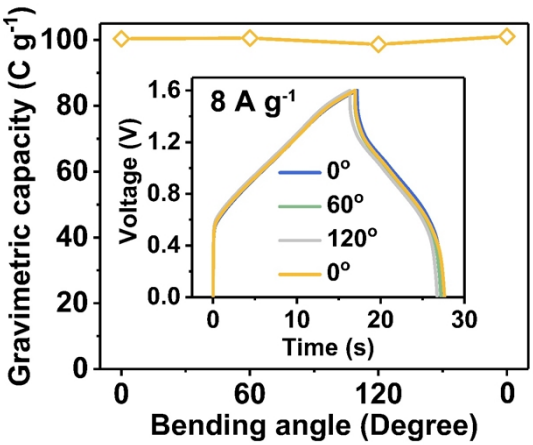

Fig. S13 Gravimetric capacities of various bending states.

References

1 M. Yi, C. Zhang, C. Cao, C. Xu, B. Sa, D. Cai and H. Zhang, *Inorg. Chem.*, 2019, **58**, 3916-3924.

2 X. Lei, S. Ge, Y. Tan, J. Li, Z. Wang, P. Liu, C. Feng and B. Xiang, *J. Mater. Chem.* A, 2019, **7**, 24908-24918.

3 H. Liang, C. Xia, Q. Jiang, A. N. Gandi, U. Schwingenschlögl and H. N. Alshareef, *Nano Energy*, 2017, **35**, 331.

4 Z. Li, H. Mi, F. Guo, C. Ji, S. He, H. Li and J. Qiu, *Inorg. Chem.*, 2021, **60**, 12197-12205.

5 S. He, F. Guo, Q. Yang, H. Mi, J. Li, N. Yang and J. Qiu, *Small*, 2021, **17**, 2100353.

6 W. Jiang, F. Hu, Q. Yan and X. Wu, *Inor. Chem. Front.*, 2017**, 4**, 1642-1648.

7 V. T. Chebrolu, B. Balakrishnan, D. Chinnadurai and H. J. Kim, *Adv. Mater. Technol.*, 2019, **5**, 1900873.

8 B. Li, P. Gu, Y. Feng, G. Zhang, K. Huang, H. Xue and H. Pang, *Adv. Funct. Mater.*, 2017, **27**, 1605784.

9 X. Li, H. Wu, A. M. Elshahawy, L. Wang, S. J. Pennycook, C. Guan and J. Wang, *Adv. Funct. Mater.*, 2018, **28**, 1800036.

10 X. Zhang, A. Wu, X. Wang, C. Tian, R. An and H. Fu, *J. Mater. Chem. A*, 2018, **6**, 17905-17914.

11 D. Chu, X. Song, L. Tan, H. Ma, H. Pang, X. Wang and D. Guo, *Inorg. Chem. Commun.*, 2019, **110**, 107587.

12 X. Liu, L. Ye, Y. Du and L. Zhao, *Mater. Lett.*, 2020, **258**, 126812.

13 R. Bendi, V. Kumar, V. Bhavanasi, K. Parida and P. S. Lee, *Adv. Energy Mater.*, 2016, **6**, 1501833.